MDPI

Article

Hygroscopicity of Waterlogged Archaeological Wood from Xiaobaijiao No.1 Shipwreck Related to Its Deterioration State

Liuyang Han [1,2], **Juan Guo** [1,2], **Kun Wang** [3], **Philippe Grönquist** [4,5], **Ren Li** [1,2], **Xingling Tian** [6] **and Yafang Yin** [1,2,*]

[1] Department of Wood Anatomy and Utilization, Research Institute of Wood Industry, Chinese Academy of Forestry, Beijing 100091, China
[2] Wood Collections (WOODPEDIA), Chinese Academy of Forestry, Beijing 100091, China
[3] College of Material Science and Technology, Beijing Forestry University, Haidian District, Beijing 100083, China
[4] Wood Materials Science, ETH Zürich, 8093 Zürich, Switzerland
[5] Laboratory for Cellulose & Wood Materials, EMPA, 8600 Dübendorf, Switzerland
[6] Heritage Conservation and Restoration Institute, Chinese Academy of Cultural Heritage, Beijing 100029, China
[*] Correspondence: yafang@caf.ac.cn; Tel.: +86-10-62889468

check for updates

Abstract: Waterlogged archaeological wood (WAW) artifacts, made of natural biodegradable polymers, are important parts of many precious cultural heritages. It is of great importance to understand the hygroscopic behavior of WAW in different deterioration states for the development of optimal drying processes and choices of safe storage in varying conditions. This was investigated in a case-study using two *Hopea* (Giam) and two *Tectona* (Teak) WAW samples collected from the Xiaobaijiao No.1 shipwreck. The deterioration state of WAW was evaluated by the maximum water content (MWC) method and by the cell morphological structure. Both *Hopea* and *Tectona* WAW could be classified into moderately and less decayed WAW. The hygroscopic behavior of moderately and less decayed WAW was then comparatively investigated using Dynamic Vapor Sorption (DVS) measurements alongside two sorption fitting models. Compositional analysis and hydroxyl accessibility measurements of WAW cell walls were shown to correlate with the hygroscopicity of WAW in different deterioration states. It was concluded that moderately decayed WAW possessed higher hygroscopicity and hysteresis than less decayed WAW because of the lower relative content of polysaccharides and the higher relative content of lignin, including the slow hydrolysis of O-acetyl groups of xylan and the partial breakage of β-O-4 interlinks, accompanied by an increased hydroxyl accessibility. This work helps in deciding on which consolidation measures are advised for shipwreck restauration, i.e., pretreatments with specific consolidates during wood drying, particularly for wooden artifacts displayed in museums.

Keywords: morphological structure; sorption behavior; sorption fitting model; compositional analysis; hydroxyl accessibility

1. Introduction

Waterlogged archaeological wooden artifacts counting as valuable cultural heritages are being excavated worldwide [1–3]. In dependence of environmental factors, wood species, period, and processed treatments, WAW excavated even from the same archaeological site or collected either from the surface or the inner part of the same wooden artifact would probably be found in different deterioration states [4–8]. In general, WAW can be divided into severely decayed wood, moderately

decayed wood, and less decayed wood [9,10]. The subdivision can be done according to maximum water content, morphological observations, and chemical structure of WAW [11–13]. Even though the water environment remarkably slows down the wood deterioration caused by microbiota, waterlogged wooden artifacts still suffer from a high possibility of deterioration. Hence, the conservation of WAW artifacts generally necessitates a water removal treatment [2,14].

Given that the two main forms of water in wood are free water in cell lumens and cell wall mesopores as well as bound water adsorbed in cell walls [7,15,16], the water-removal treatment incorporates both removal of free water and desorption of bound water. The treatment may lead to cell morphology changes due to surface tension that affect the dimensional stability of archaeological wooden artifacts because of cell wall shrinkage and collapse [15,17–20]. The sorption of bound water relies on the hygroscopic behavior of WAW, which is related to the dimensional instability that causes cracks and distortions in WAW [21]. Previous works have found that buried archaeological wood possesses a higher equilibrium moisture content (EMC) and higher hysteresis coefficients than recent wood [22,23], which could be attributed to the deacetylation of hemicelluloses, the degradation of amorphous celluloses, and a decrease of crystallinity. Moreover, WAW possesses varying deterioration states, each of which features an inhomogeneous deterioration behavior [24] and may require specific water-removal treatment to avoid unnecessary damage caused by cell wall shrinkage. Thus, it is of great importance to understand the hygroscopic response of WAW to different deterioration states in order to develop optimal drying processes, suitable display conditions, and safe storage under varying climatic conditions [25,26]. However, no studies yet illustrate the influence of deterioration state of WAW on its hygroscopicity.

The aim of this work is to compare the hygroscopicity of WAW in different deterioration states and to provide basic knowledge for their preservation, particularly in terms of the selection of drying method and storage conditions. Herein, two hardwood species of WAW, *Hopea* (Giam) and *Tectona* (Teak), were collected from the marine Xiaobaijiao No.1 shipwreck dated as 1821–1850 [27,28]. MWC and observation of cell morphological structure by LM and SEM were adopted to classify the deterioration state of WAW. The hygroscopic behavior was then examined by DVS, including analysis of equilibrium moisture content (EMC) and sorption hysteresis, and by fitting sorption/desorption curves with two frequently used multilayer sorption models; the Guggenheim, Anderson, and De Boer (GAB) and the Generalized D'Arcy and Watt (GDW) models. Furthermore, deuterium exchange measurements were conducted in order to gain information regarding the hydroxyl group accessibility. And finally, the study was complemented by compositional analysis in order to better understand the effect of cell wall degradation on the hygroscopicity of WAW.

2. Materials and Methods

The Xiaobaijiao No.1 shipwreck, now preserved in a waterlogged environment at the Ningbo Base of the Chinese National Center of Underwater Cultural Heritage (Ningbo, China), was a commercial ship in the period from 1821 to 1850 AD. The wreck site (scheme as shown in Figure 1) is located on Yushan Island, China [27]. Considering that an ideal selection of the reference wood specimens is a challenge for the comparison with the broader archaeological wood research, two samples corresponding to each of the two species composing the shipwreck were carefully chosen for comparable results. The locations of four samples (denoted H1, H2, T1, and T2) collected for this study are marked in Figure 1 and the detailed position information is listed in Table 1. Samples H1 and H2 were identified as *Hopea* spp. (Giam), while T1 and T2 were identified as *Tectona* spp. (Teak). As reported by a previous and related publication [28], the maximum water content (MWC) of the samples H1, H2, T1 and T2 were 121.59% ± 16.7%, 264.43% ± 80.55%, 108.51% ± 4.5% and 189.59% ± 65.36%, respectively.
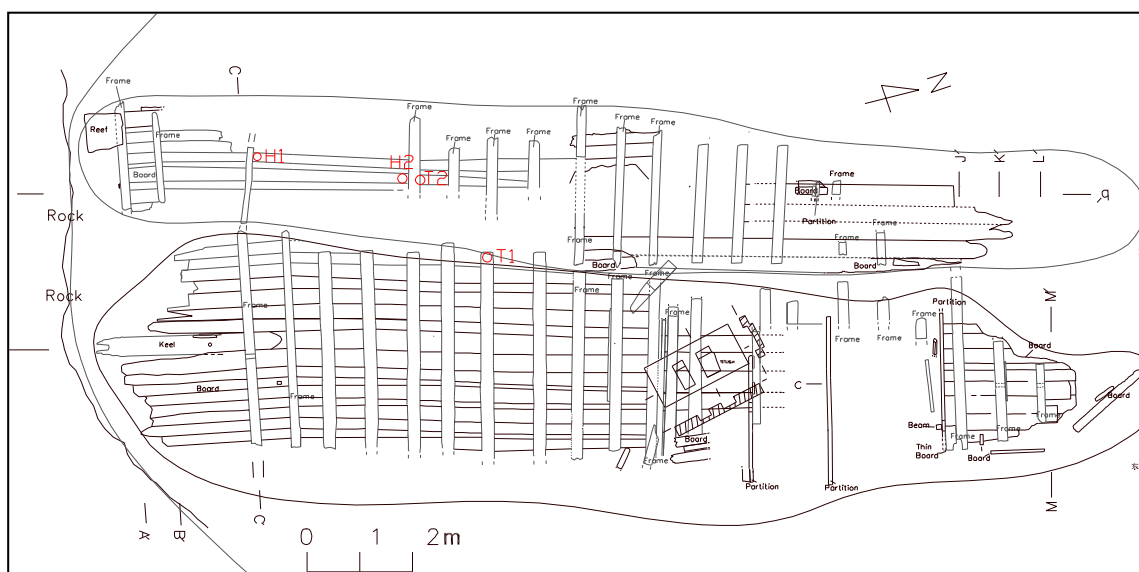
Figure 1. Scheme of the Xiaobaijiao No.1 shipwreck with the sample locations marked in red. *Hopea* WAW: H1, H2; *Tectona* WAW: T1, T2.

Table 1. Detailed position of the samples collected from the Xiaobaijiao No.1 shipwreck.

Sample Name	Sampling Position
H1	The 5th inner layer board of the hull
H2	The 4th inner layer board of the hull
T1	The 6th inner layer board of the hull
T2	The 7th inner layer frame of the hull

2.1. LM

Cross sections of *Hopea* and *Tectona* WAW were prepared by a rotary microtome (RM 2255, Leica, Wetzlar, Germany) with a thickness of 10 μm. A light microscope (BX51, Olympus, Tokyo, Japan) was used to examine microstructure of the specimens.

2.2. SEM

Prior to the SEM examination, all cross-section surfaces of WAW were prepared by a rotary microtome (RM M2255, Leica, Germany). To avoid creating artificial damage to the cell wall structure during cutting with the microtome, the WAW samples were embedded with polyethylene glycol (PEG) 2000 (average molecular mass: 1900–2200 g/mol), which was followed by a rinsing process under flowing water for 30 min to remove the PEG. After mounting the dry samples on aluminum stubs followed by a sputter-coating process with Platinum, the samples were observed using a field emission scanning electron microscope (Quanta 200F FEI, Thermo Fisher Scientific, Waltham, MA, USA) at a voltage of 10 kV.

2.3. DVS

EMC of moderately decayed and less decayed WAW in different relative humidity (RH) states were measured by an automated sorption balance device (DVS Advantage ET85, Surface Measurement Systems Ltd., Wembley, UK). Measurements were mainly conducted according to the protocol found in [29]. Samples were cut into millimeter thick stripes by a razor blade and 30 mg of the waterlogged stripes were initially dried at a partial water vapor pressure of $p/p_0 = 0$ for 600 min. The samples were then exposed to ascending p/p_0 steps ranging from 0 to 0.98 for adsorption and then descending in the same manner for desorption at 25 °C. Equilibrium in each step was defined to be reached at a mass

change per time (dm/dt) of less than 0.0005%/min over a 10 min stability window or a maximal time of 1000 min per step. The sorption hysteresis parameters were calculated by the difference of EMC for desorption and adsorption in the same relative humidity.

2.4. Isotherm Models

The obtained isotherms by DVS were fitted with two common sorption models, whose parameters were obtained by least-square fits to the data for each sample. The first of the models, the GAB model, was mainly improved from the commonly used BET isotherm model by increasing the sorbate activity range [30], and was first recommended by the European Project Group COST 90 [31] as a fundamental equation to characterize water sorption in food. It was subsequently introduced for the analysis of wood [7,32,33]. The GAB equation reads as:

$$\mathrm{EMC} = \mathrm{M_m} \frac{\mathrm{K_{GAB} \cdot C_{GAB} \cdot RH}}{(1 - \mathrm{K_{GAB} \cdot RH}) \cdot (1 - \mathrm{K_{GAB} \cdot RH} + \mathrm{C_{GAB} \cdot K_{GAB} \cdot RH})} \times 100\% \qquad (1)$$

where *EMC* (%) is the equilibrium moisture content; *RH* (%) is the air relative humidity; M_m is the monolayer capacity; C_{GAB} (%) is the equilibrium constant related to the monolayer sorption, and K_{GAB} (%) is the equilibrium constant related to the multilayer sorption.

In addition, the internal specific surface area (S_{GAB}) of WAW can be obtained based on the values of Mm provided by the GAB model:

$$\mathrm{S_{GAB}} = \frac{\mathrm{M_m \cdot \rho \cdot L \cdot \sigma}}{\mathrm{M}} \qquad (2)$$

where ρ is the density of water, L is the Avogadro number, σ is the average area where water occupies the complete monolayer (0.114 nm^2 was used in this study for the surface area occupied by a single water molecule) and M is the molar mass of water [26,34].

The second isotherm model used, the GDW model, assumes that the Langmuir mechanism governs the monolayer sorption, i.e., only one water molecule can be directly bound to a primary sorption site and that there are three possible scenarios: (a) the number of the secondary sites is lower than the number of primary sites (i.e., primary bound water molecules are not completely converted into the secondary sorption sites, *w* < 1. *w* is a conversion ratio of primary bound water molecules into the secondary sites); (b) the number of the secondary sites is equal to the primary sites (i.e., each monolayer molecule is converted into the secondary site, *w* = 1); (c) the number of the secondary sites is higher than the primary sites (i.e., each primary bound molecules creates more than one secondary sorption site, *w* > 1) [32].The GDW model [32,35] equation reads as:

$$\mathrm{EMC} = \frac{\mathrm{m_{GDW} \cdot K_{GDW} \cdot RH}}{(1 + \mathrm{K_{GDW} \cdot RH})} \cdot \frac{1 - \mathrm{k_{GDW}}(1 - w) \cdot \mathrm{RH}}{(1 - \mathrm{k_{GDW} \cdot RH})} \times 100\% \qquad (3)$$

where m_{GDW} (%) is the maximum amount of water bound to the primary sorption sites, i.e., the monolayer water content. K_{GDW} (%) is a constant of sorption kinetics on the primary sites, and k_{GDW} (%) is a constant of sorption kinetic on the secondary sites.

2.5. Compositional Analysis

The carbohydrates and total lignin of WAW specimens were measured with 3 replicates under the standard procedure according to the National Renewable Energy Laboratory (NREL, Golden, CO, USA) protocol [36,37]. Briefly, the milled specimens were hydrolyzed in 72% H_2SO_4 for 1 h at 30 °C and were then completely hydrolyzed in an autoclave at 121 °C for 1 h. The acid insoluble lignin was determined by weighing the solid, and the monosaccharides in the liquid were detected by high-performance anion exchange chromatography (Dionex ISC 3000, Sunnyvale, CA, USA).

2.6. Hydroxyl Accessibility

The WAW samples measured by DVS were further used to study the hydroxyl accessibility. The samples, initially dried at $p/p_0 = 0$ and 40 °C for 6 h, were exposed to D_2O vapor at $p/p_0 = 0.95$ and 25 °C for 10 h to ensure that the material's accessible hydrogen protium is completely replaced by deuterium [38]. Then, the drying procedure was applied again, and the deuterated dry mass m_D was obtained. The number of available water vapor accessible OH groups (sorption sites) was calculated by equation (3) [29,39]:

$$\text{Number} = \frac{m_D - m_{\text{dry}}}{m_{\text{dry}} \cdot (M_D - M_H)} \tag{4}$$

where m_{dry} is the dry mass of archaeological wood; M_D is the molar mass of deuterium and M_H is the molar mass of protium.

3. Results and Discussion

3.1. The Deterioration State of Waterlogged Archaeological Wood

According to the MWC values, the most commonly used parameter to classify the deterioration state of waterlogged archaeological wood [9,10], samples H2 and T2 belong to class of moderately decayed wood (185% < MWC < 400%), while H1 and T1 can be regarded as class of less decayed wood (MWC<185%). LM and SEM revealed the morphological structures of the WAW specimens and confirmed these deterioration states [6,9]. Cells in H1 mainly remained intact (Figure 2A) without significant deterioration features visible in the SEM image (Figure 3A). In contrast, the morphological structure of cell walls in H2 displayed pronounced decay patterns (Figure 2C). Parts of the S_2 layers and the S_3 layers of the fiber cell walls were degraded (Figure 3C), which is a sign of erosion bacteria decay pattern [24]. Furthermore, some parts of the cell walls of sample H2 were depleted by microbiological degradation with significant cavities emerging. Similar micro-morphological structure differences were present in T1 and T2. As for less decayed waterlogged *Tectona* (T1), the morphology shown by LM (Figure 2B) and SEM (Figure 3B) also indicated no pronounced sign of degradation. However, obvious features of soft-rot decay [24] were found in T2 by both LM (Figure 2D) and SEM (Figure 3D). Specifically, the S_3 layers of the cell walls of T2 were still intact, while cavities occurred in its S_2 layers. To sum up, the two moderately decayed WAWs were deteriorated to some degree by microorganisms with pronounced alternations of their cell morphologies, while the two less decayed WAWs in this research didn't show any obvious cell morphologies indicating decay. Thus, the deterioration states of *Hopea* and *Tectona* WAW revealed by the morphological method were well consistent with the MWC method in this study.
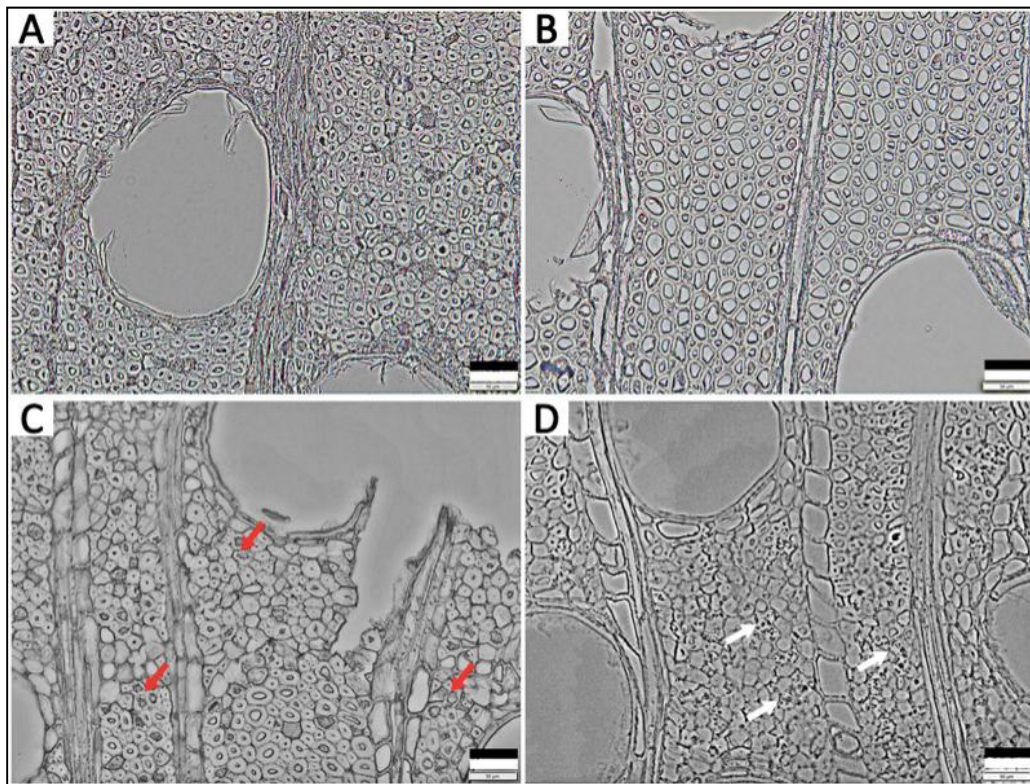
Figure 2. Light microscopy images of *Hopea* waterlogged archaeological wood (WAW): H1 (**A**): Less decayed sample, H2 (**C**): Moderately decayed sample (red arrows display pronounced decay patterns indicating degraded fiber cell walls); *Tectona* WAW: T1 (**B**), Less decayed sample, T2 (**D**): Moderately decayed sample (white arrows show that cavities occurred in its S_2 layers indicate degraded fiber cell walls). Scale bar = 50 μm.
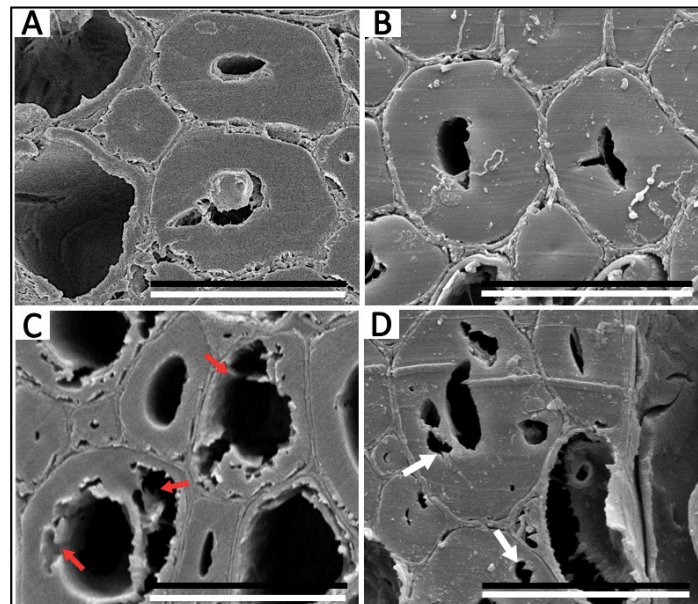
Figure 3. SEM images of *Hopea* WAW: H1 (**A**): Less decayed sample, H2 (**C**): Moderately decayed sample (red arrows indicate decay in the S_2 and in many of the S_3 layers within the fiber cell walls); *Tectona* WAW: T1 (**B**): Less decayed sample, T2 (**D**): Moderately decayed sample (white arrows indicate cavities visible in the S_2 layers). Scale bar = 20 μm.

3.2. Hygroscopicity of WAW in Different Deterioration States

The sorption isotherms of *Hopea* and *Tectona* WAW in different deterioration states are shown in Figure 4 for a single adsorption and desorption cycle per sample. All adsorption and desorption curves display S-shapes, which implies that the sorption isotherms of both moderately and less decayed WAW might be classified as type IV IUPAC isotherms [40–44] (Whether the measured isotherms can be classified as type II or type IV can be debated. Some studies [41,43,44] classified wood sorption isotherms as type II, but this depends on the chosen interpretation of the sorption mechanisms; either exclusively mono/multilayer adsorption, or a mix with capillary condensation in mesopores of the cell wall [40]. Here the authors assume type IV.). The sorption isotherms of all specimens exhibited an upward bend at around 60%–80% RH, which is commonly reported in lignocellulosic materials [26,32,43]. Furthermore, the EMCs of moderately decayed WAW at each RH were all higher than those of less decayed WAW. At the highest relative humidity (98% RH), the EMCs of H2 and T2 reached as high as 25.91% and 27.37%, whereas the EMC of H1 and T1 reached 21.55% and 22.15%, respectively. Furthermore, different relative changes in EMCs (M_m/M_l) in both adsorption and desorption branches were present for both *Hopea* and *Tectona* WAW. The EMCs in both adsorption and desorption of H2 were at least 15% higher than those of H1 (Figure 5A). As for *Tectona*, the EMCs in adsorption for T2 were 19% to 39% higher than those of T1, and the EMCs in desorption for the former were 20%–49% higher than the latter (Figure 5B).
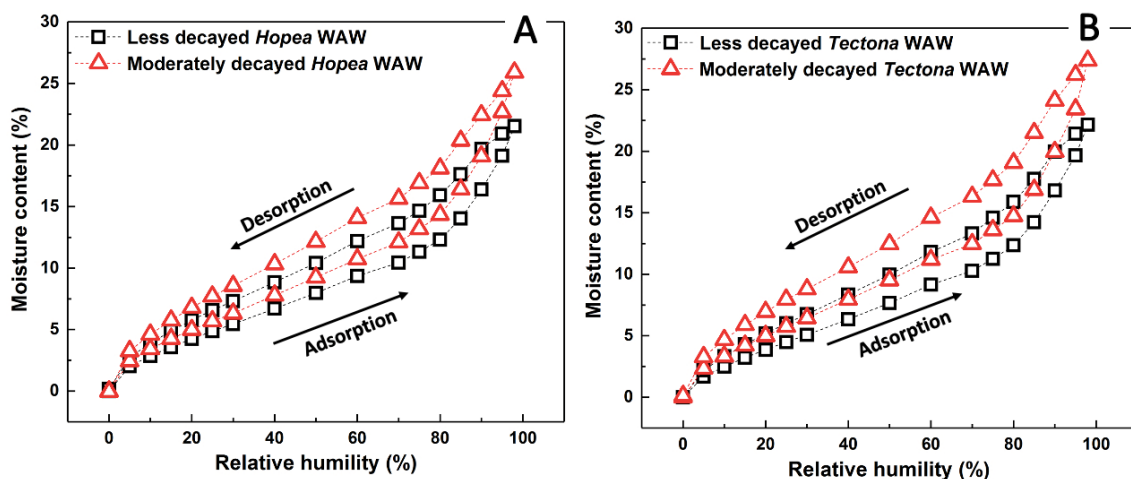
Figure 4. Equilibrium moisture content (EMC) of *Hopea* (**A**) and *Tectona* (**B**) WAW. Water vapor adsorption and desorption curves for the less decayed (H1 and T1, open black squares) and the moderately decayed (H2 and T2, open red triangles) samples.

In addition to the increase of EMCs, sorption hysteresis of moderately decayed WAW was also higher than that of less decayed WAW. The sorption hysteresis is commonly calculated as the difference between adsorption and desorption branches of an isotherm in the range between the highest relative humidity (98% RH) and 0% RH [45]. It is believed to originate from a potential rearrangement of structural components in cell walls [46]. As shown in Figure 6, sorption hysteresis indeed exists in the whole moisture extent from 0% RH to 98% RH. The measurable sorption hysteresis of moderately decayed WAW was found higher than that of less decayed WAW at every humidity condition and for both *Hopea* and *Tectona* WAW. The higher sorption hysteresis of moderately decayed WAW as compared to less decayed WAW might lead to the higher variation in surface moisture content of wood elements under standard changes of relative humidity [46]. Therefore, conservators of archaeological artifacts usually try to consolidate WAW, for example, with lactitol and trehalose, in order to lower the sorption hysteresis [32,47].
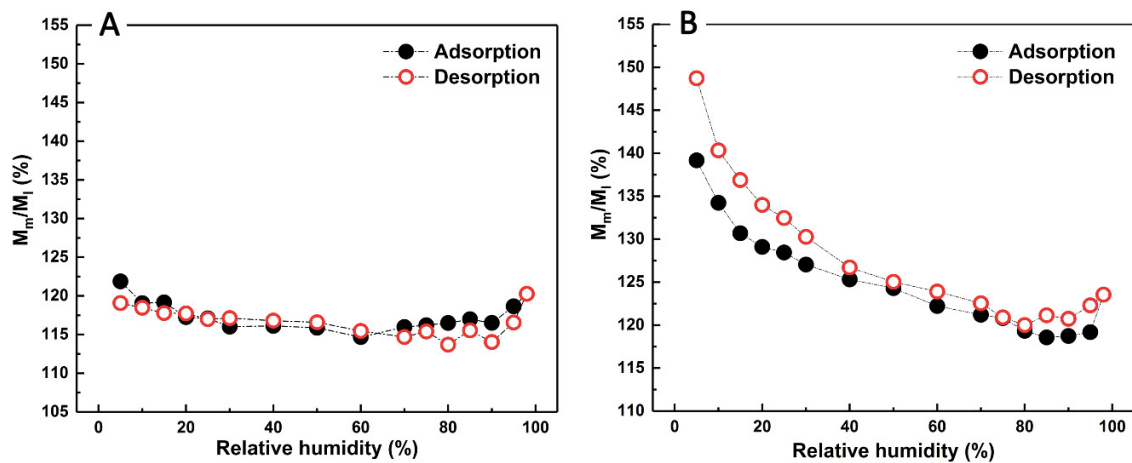
Figure 5. Relative changes in EMCs (M_m/M_l) in adsorption (black solid cycles) and desorption (red open cycles) of *Hopea* (**A**) and *Tectona* (**B**) WAW. M_m = moisture content (MC) of moderately decayed WAW (H2, T2); M_l = MC of less decayed WAW (H1, T1).
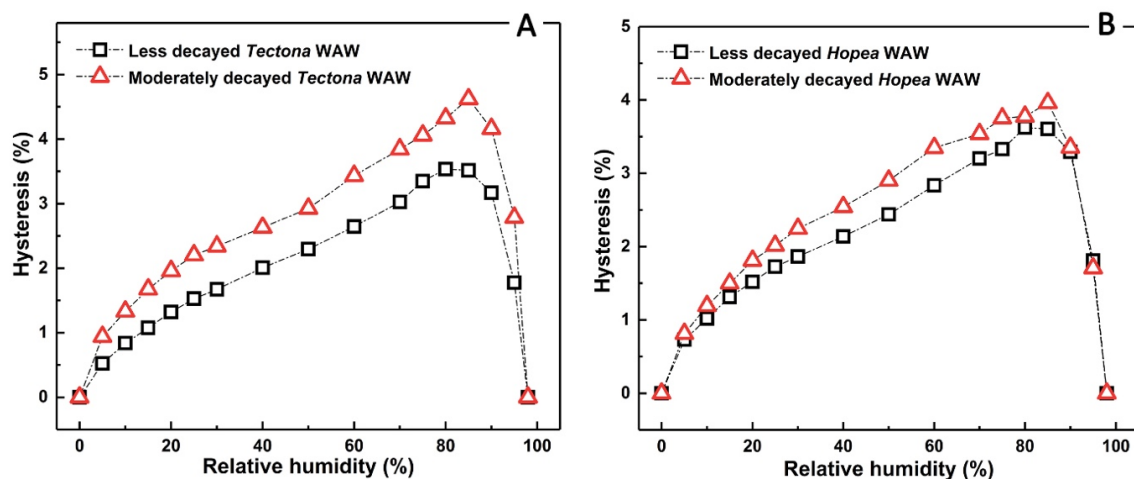
Figure 6. Sorption hysteresis of *Hopea* (**A**) and *Tectona* (**B**) WAW for the less decayed (H1, T1, open black squares) and the moderately decayed (H2, T2, open red triangles) samples.

In order to analyze the sorption process in detail, GAB and GDW sorption models were applied to fit the adsorption and desorption isotherms of *Hopea* and *Tectona* WAW with two deterioration states. The fits were considered to be valid if all the coefficient of determination (R^2) values were above 0.99 [26,48]. The parameters calculated by a least-square fitting were listed in Table 2.

With the analysis by the GAB model, as listed in Table 2, it could be noticed that the C_{GAB} values were approximately an order of magnitude higher than the K_{GAB} values for all samples, indicating much higher heat of sorption of the monolayer as compared to the multilayer [49]. It could also be deduced from the GAB model that the necessary condition for classifying the isotherms as type II (in this context, the authors assume that the sorption isotherm is the result of unrestricted mono/multilayer adsorption up to high p/p_0) was satisfied because the conjunction of the relations $5.57 \leq C_{GAB} < \infty$ and $0.24 < K_{GAB} \leq 1$ was satisfied for the analyzed isotherms [32,50]. The maximum monolayer water content reflected by the M_m coefficient was found 11.74% higher for H2 than the M_m for H1. For *Tectona* WAW it was found 16.74% higher during the adsorption processes. For the desorption processes, the value for H2 was 8.80% higher than that of H1 and in the case of *Tectona*, it was 13.29% higher. The increased maximum monolayer water contents for moderately decayed WAW imply that long-time deterioration increased the number of accessible primary sorption sites compared to less decayed WAW. Besides, the M_m coefficient is proportional to the internal specific surface area

(S_{GAB}) [26,34], from which can be deduced that the internal specific surface area of WAW increases with the deterioration level. It was found that the C_{GAB} coefficient, which represents the total heat of sorption of the monolayer water [26,51], was higher for moderately decayed WAW than that for less decayed WAW. The C_{GAB} coefficients for H2 were 16.48% and 17.91% higher than those of H1, and in the case of *Tectona* they were 40.88% and 49.31% higher for both the adsorption and desorption processes respectively. These results could lead to the interpretation that the monolayer water is bound more strongly to the primary sorption sites for moderately decayed WAW as compared to less decayed WAW.

Table 2. Coefficients of the GAB and GDW models for *Hopea* and *Tectona* WAW in different deterioration states.

Sample	Sorption Phase	GAB Model					GDW Model				
		M_m	K_{GAB}	C_{GAB}	R2	S_{GAB}	m_{GDW}	K_{GDW}	k_{GDW}	w	R2
H1	Adsorption	4.94	0.79	15.59	0.999	187.68	8.70	4.41	0.86	0.39	1
	Desorption	8.30	0.66	10.72	1	315.34	6.69	11.32	0.58	1.97	1
H2	Adsorption	5.52	0.80	18.16	0.999	209.72	9.74	4.86	0.87	0.39	1
	Desorption	9.03	0.68	12.64	1	343.08	9.60	8.23	0.67	1.04	1
T1	Adsorption	4.84	0.80	11.79	1	183.88	8.57	3.71	0.85	0.45	1
	Desorption	8.20	0.67	8.01	1	311.54	6.62	8.38	0.61	1.90	1
T2	Adsorption	5.65	0.81	16.63	0.999	214.66	11.55	3.64	0.88	0.31	1
	Desorption	9.29	0.69	11.96	0.999	352.96	9.20	9.12	0.67	1.22	0.999

Note: M_m (%) is the monolayer capacity, C_{GAB} (%) is the equilibrium constant related to the monolayer sorption, K_{GAB} (%) is the equilibrium constant related to the multilayer sorption, S_{GAB} (m^2/g) is the internal specific surface area, m_{GDW} (%) is the maximum amount of water bound to the primary sorption sites, i.e., the monolayer water content, K_{GDW} (%) is a constant of sorption kinetic on the primary sites, k_{GDW} (%) is a constant of sorption kinetic on the secondary sites, w – conversion ratio of primary bound water molecules into the secondary sites.

Using the GDW model, the maximum content of water bound to primary sites (m_{GDW}) of H2 was 11.95% higher than that of H1, and in the case of *Tectona* WAW 34.77%, during the adsorption processes. During desorption processes, the m_{GDW} of the H2 sample was 43.50% higher than for H1, and in the case of *Tectona*, it was 38.97% higher. This could indicate an increased number of primary sorption sites for water in moderately decayed WAW. The ratio of water molecules bound to primary sites and converted into secondary sites (w) of WAW generally decreased with deterioration state. The values of H1 and H2 were the same. During the desorption processes, for *Tectona*, the value of T2 was 31.11% less than that of T1 during the adsorption. The value of H2 was 47.21% less than that of H1, and the in the case of *Tectona*, it was 35.79% less. The results would imply that each primary bound molecule of moderately decayed WAW created less secondary sorption sites than in the case of less decayed WAW. However, the decreased w of WAW in this study and other related studies [32,46] did not obviously contribute to the increased hygroscopicity because of the significant contribution of the increased number of primary sorption sites.

The GAB and the GDW sorption models both indicated that moderately decayed WAW may possess more sorption sites and display a stronger capability of adsorbing water vapor from the surrounding environment than less decayed WAW.

3.3. The Chemical Deterioration and Increased Hydroxyl Accessibility of Waterlogged Archaeological Wood

The hygroscopicity of wood highly depends on the relative contents of the main components in the cell wall, i.e., cellulose, hemicellulose, and lignin [52]. The results of the compositional analysis of WAW in different deterioration states are shown in Table 3. The amount of cellulose, the most significant component, is reflected by the relative content of glucose. The content of hemicellulose can be assigned to the relative content of xylose, because in hardwoods, xylan dominates the composition of hemicellulose [52]. Finally, the Klason lignin content was used to reflect the content of lignin [53].

Table 3. Chemical compositions of WAW collected from the Xiaobaijiao No.1 shipwreck. Chemical composition 100% means related to investigated components. Statistics for n = 3 measurements. The standard deviations were less than 2%.

Sample	Acid-Insoluble Lignin	Acid-Soluble Lignin	Glucose	Xylose
H1	46.0%	1.0%	45.6%	7.4%
H2	55.8%	1.0%	39.3%	3.9%
T1	45.0%	0.8%	47.6%	6.6%
T2	54.6%	0.8%	38.8%	5.8%

For H2, the relative content of cellulose counted by the proportion of glucose is 39.2% (according to total dry weight), 14% lower than that of H1. Xylose accounted for 3.9%, which was 47.3% lower than in the case of H1. In contrast, the relative content of lignin was 56.6% (55.6% Klason lignin and 1% acid-soluble lignin) for H2, 21% higher than that of H1. Additionally, it was found that the relative content of Klason lignin decreased from 55.6% to 46% from H2 compared to H1. As stated, the increased content of lignin in moderately decayed WAW does not indicate an absolute increase of lignin during the long-term deterioration process, instead, this is mainly a result from the loss of polysaccharides including hemicelluloses and cellulose [54]. For *Tectona* WAW, the compositional analysis presented the same tendency with a 9.6% higher lignin content and a 9.8% lower glucose content as well as a 0.8% lower xylose content for moderately decayed compared to less decayed WAW.

The increase of EMC for the WAW can be understood in terms of the increase of both the number of sorption sites and their accessibility, as reported by a previous and related publication, where it was shown that the changes of chemical and cellulose crystallite structure led to an increased bound water uptake [7]. The hydroxyl accessibility of WAW was obtained in this work to further explore the apparent difference in hygroscopicity between moderately decayed and less decayed WAW.

Figure 7 displays the number of accessible hydroxyl groups obtained by sample deuteration using heavy water. The amount of accessible hydroxyl groups of wood generally ranges from 6.8–10.3 mmol/g according to previous research [38,55]. In this study, the number of accessible hydroxyl groups of H2 was 7.5 ± 0.4 mmol/g, while that of H1 was lower, with a value of 6.8 ± 0.3 mmol/g. For *Tectona* WAW, T2 showed a higher mean value of 7.9 ± 0.5 mmol/g, while T1 showed a lower accessibility of 7.0 ± 0.5 mmol/g. Because the amount of available OH groups is generally believed to directly correlate with the amount of sorption sites, the 10% and 13% higher numbers of hydroxyl groups in moderately decayed WAW could strongly indicate why the EMCs and hysteresis were higher in moderately decayed WAW than for less decayed WAW.

The observed changes in hydroxyl accessibility could be either attributed to alternation of structure or to changes of chemical composition [29,56] upon deterioration. In fact, lignin, hemicellulose, and cellulose possess different amounts of hydroxyl groups [57], and as was reported above, they were each found to degrade to some different extent in WAW. The compositional analysis of different substrates revealed that the deterioration of WAW was mainly related to the decomposition of polysaccharides in the cell wall. Cellulose and hemicelluloses are in general extensively affected by anaerobic microorganisms and by occurring acid or alkali environment conditions [5] during the 170-years deterioration in waterlogged conditions. It is known that slow hydrolysis of O-acetyl groups of xylan always occurs in decayed archaeological hardwood [22,58,59]. As the hemicellulose is the most hydrophilic polymer in wood, its degradation generally results in a reduced hygroscopicity [60]. However, it should be emphasized that the hygroscopicity was higher for WAW than recent wood although the hemicellulose of WAW was severely degraded compared to cellulose and lignin, as illustrated by previous studies [7,32,47]. As shown in Table 3, the relative content of xylose representing hemicellulose decreased a lot. That means that besides hemicellulose, variations in the component structures of cellulose and lignin should also contribute to the increased hygroscopicity of WAW. Besides hemicellulose, cellulose is also considered as a major substance contributing to the hydrophilicity of wood and of other natural biodegradable polymers [61–63]. Although the interior of

the cellulose microfibrils is not accessible to water vapor [64], the hydroxyl groups on surface chains are accessible [65–67]. Furthermore, the extent of moisture sorption of cellulose was reported to increase with decreasing degree of crystallinity [61,68]. In WAW, the deterioration of cellulose includes both the degradation of amorphous cellulose and the decrease of relative crystallinity [23,69]. In this research, the observed decrease of relative content of cellulose could demonstrate its degradation, and in addition, changes in amorphous cellulose and crystallinity were reported in the related previous study [69]. Therefore, both aspects might explain the observed increase in hygroscopicity. However, next to the deterioration of cellulose and hemicellulose, the modification of lignin may also lead to an increase of adsorbent functional groups in WAW [7,54,69], responsible for an increased uptake of water vapor. In detail, lignin in archaeological wood generally undergoes modifications such as the partial breakage of β-O-4 interlinks, an alternation of lignin structure, and demethylation/demethoxylation [7,54,70,71]. Although there is few studies on the relationship between WAW and the number of available OH groups, it was reported that the amount of available OH groups of delignified wood increased with the degree of delignification [29]. Both WAW and delignified wood possesses more OH groups because their lignin appears to be less bound to the carbohydrate matrix, enabling a flexible conformation. Additionally, the structure of lignin was partly altered, similar to extracted lignin [29,69]. In the current study, the increase in relative content of lignin of moderately decayed WAW (shown in Table 3) was caused by the loss of cellulose and hemicellulose, which implied that the lignin must have been modified to some degree throughout the deterioration in order to explain the increased hygroscopicity. To sum up, the demonstrated increase of hygroscopicity in more decayed WAW can be attributed to changes of relative components of the cell wall. It could be demonstrated that interpretations regarding hygroscopicity can correlate well between compositional analysis and hydroxyl accessibility measurements.
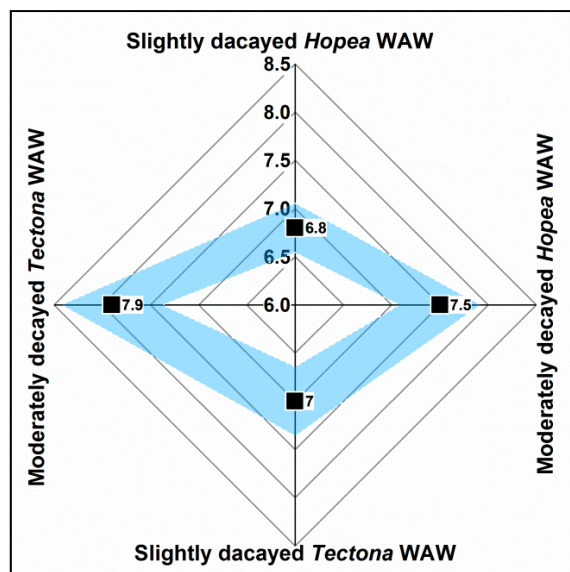
Figure 7. Radar image of the number (mmol/g) of accessible hydroxyl groups of the less decayed (H1, T1) and the moderately decayed (H2, T2) samples. The mean values (black squares) and the standard deviation (blue bands) were calculated from statistics for n = 3 measurements using representative samples.

4. Conclusions

Two hardwood species of waterlogged archaeological wood, *Hopea* and *Tectona*, were collected from a 170-year-old shipwreck, the Xiaobaijiao No.1, in order to investigate the effect of the deterioration on the hygroscopicity. Two deterioration states i.e., moderately decayed and less decayed WAW were confirmed by LM and SEM. In terms of water vapor sorption, moderately decayed WAW showed the higher EMCs and hysteresis than less decayed WAW. The fitted sorption models revealed that, towards

WAW, the monolayer water was bound more strongly to primary sorption sites and the number of primary sorption sites increased with deterioration. The observed increase in hygroscopicity was attributed to a more severe deterioration of the wood chemical components of moderately decayed WAW in contrast to the less decayed WAW. In addition to higher hygroscopicity, moderately decayed WAW showed higher hysteresis than less decayed WAW, particularly above 60% RH, which is a domain close to museum humidity conditions (50%–60% RH for wooden artifacts in China). Therefore, considering the irreversible alternations in chemistry of WAW, the active reduction of sorption sites of WAW could be recommended as a possible strategy for conservation. Differentiated and appropriate conservation treatments would be required for WAW in different deterioration states.

References

1. Seborg, R.M.; Inverarity, R.B. Preservation of old, waterlogged wood by treatment with polyethylene glycol. *Science* **1962**, *136*, 649–650. [CrossRef] [PubMed]

2. Walsh-Korb, Z.; Avérous, L. Recent developments in the conservation of materials properties of historical wood. Prog. *Mater. Sci.* **2019**, *102*, 167–221.

3. Sandström, M.; Jalilehvand, F.; Persson, I.; Gelius, U.; Frank, P. Deterioration of the seventeenth-century warship Vasa by internal formation of sulphuric acid. *Nature* **2002**, *415*, 893–897.

4. Hoffmann, P.; Singh, A.; Kim, Y.S.; Wi, S.G.; Kim, I.-J.; Schmitt, U. The Bremen Cog of 1380–an electron microscopic study of its degraded wood before and after stabilization with PEG. *Holzforschung* **2004**, *58*, 211–218. [CrossRef]

5. Bjurhager, I.; Halonen, H.; Lindfors, E.L.; Iversen, T.; Almkvist, G.; Gamstedt, E.K.; Berglund, L.A. State of degradation in archeological oak from the 17th century Vasa ship: Substantial strength loss correlates with reduction in (holo)cellulose molecular weight. *Biomacromolecules* **2012**, *13*, 2521–2527. [CrossRef] [PubMed]

6. Macchioni, N.; Pizzo, B.; Capretti, C.; Giachi, G. How an integrated diagnostic approach can help in a correct evaluation of the state of preservation of waterlogged archaeological wooden artefacts. *J. Archaeol. Sci.* **2012**, *39*, 3255–3263. [CrossRef]

7. Guo, J.; Xiao, L.; Han, L.; Wu, H.; Yang, T.; Wu, S.; Yin, Y.; Donaldson, L.A. Deterioration of the cell wall in waterlogged wooden archeological artifacts, 2400 years old. *IAWA J.* **2019**, *1*, 1–25. [CrossRef]

8. Macchioni, N.; Pizzo, B.; Capretti, C. An investigation into preservation of wood from Venice foundations. *Constr. Build. Mater.* **2016**, *111*, 652–661. [CrossRef]

9. Macchioni, N.; Capretti, C.; Sozzi, L.; Pizzo, B. Grading the decay of waterlogged archaeological wood according toanatomical characterisation. The case of the Fiavé site (N-E Italy). *Int. Biodeter. Biodegr.* **2013**, *84*, 54–64. [CrossRef]

10. De Jong, J. Conservation techniques for old waterlogged wood from shipwrecks found in the Netherlands. Biodeterior. *Invest. Tech.* **1977**, *113*, 295–338.

11. Babiński, L.; Izdebska-Mucha, D.; Waliszewska, B. Evaluation of the state of preservation of waterlogged archaeological wood based on its physical properties: Basic density vs. wood substance density. *J. Archaeol. Sci.* **2014**, *46*, 372–383. [CrossRef]

12. Broda, M.; Mazela, B.; Krolikowska-Pataraja, K.; Siuda, J. The state of degradation of waterlogged wood from different environments. *Ann. Wars. Univ. Life Sci. SGGW For. Wood. Technol.* **2015**, *91*, 23–27.

13. Irbe, I.; Bikovens, O.; Fridrihsone, V.; Dzenis, M. Impact of biodeterioration on structure and composition of waterlogged foundation piles from Riga Cathedral (1211 CE), Latvia. *J. Archaeol. Sci. Rep.* **2019**, *23*, 196–202. [CrossRef]

14. Walsh, Z.; Janeček, E.R.; Hodgkinson, J.T.; Sedlmair, J.; Koutsioubas, A.; Spring, D.R.; Welch, M.; Hirschmugl, C.J.; Toprakcioglu, C.; Nitschke, J.R. Multifunctional supramolecular polymer networks as next-generation consolidants for archaeological wood conservation. *Proc. Natl. Acad. Sci. USA* **2014**, *111*, 17743–17748. [CrossRef] [PubMed]

15. Skaar, C. *Wood-Water Relations*; Springer Science & Business Media: Heidelberg, Germany, 2012.

16. Zhan, T.; Jiang, J.; Lu, J.; Zhang, Y.; Chang, J. Frequency-dependent viscoelastic properties of Chinese fir (*Cunninghamia lanceolata*) under hygrothermal conditions. Part 1: Moisture adsorption. *Holzforschung* **2019**, *73*, 727–736. [CrossRef]

17. Choong, E.T.; Achmadi, S.S. Effect of extractives on moisture sorption and shrinkage in tropical woods. *Wood Fiber Sci.* **2007**, *23*, 185–196.

18. Rowell, R.M.; Banks, W.B. *Water Repellency and Dimensional Stability of Wood*; Gen. Tech. Rep. FPL-50; US Department of Agriculture, Forest Service, Forest Products Laboratory: Madison, WI, USA, 1985; 24p.

19. Fackler, K.; Schwanninger, M. Accessibility of hydroxyl groups of brown-rot degraded spruce wood to heavy water. *J. Near Infrared Spec.* **2011**, *19*, 359–368. [CrossRef]

20. Rowell, R. *Protection of Wood Against Biodegradation by Chemical Modification*; Ellis Horwood: Hemel Hempstead, UK, 1993.

21. Thybring, E.E.; Glass, S.V.; Zelinka, S.L. Kinetics of Water Vapor Sorption in Wood Cell Walls: State of the Art and Research Needs. *Forests* **2019**, *10*, 704. [CrossRef]

22. Esteban, L.G.; de Palacios, P.; Fernández, F.G.; Guindeo, A.; Conde, M.; Baonza, V. Sorption and thermodynamic properties of juvenile Pinus sylvestris L. wood after 103 years of submersion. *Holzforschung* **2008**, *62*, 745–751. [CrossRef]

23. Esteban, L.G.; de Palacios, P.; Fernández, F.G.; Martín, J.A.; Génova, M.; Fernández-Golfín, J.I. Sorption and thermodynamic properties of buried juvenile Pinus sylvestris L. wood aged 1,170±40 BP. *Wood Sci. Technol.* **2009**, *43*, 679–690. [CrossRef]

24. Singh, A.P.; Kim, Y.S.; Chavan, R.R. Relationship of wood cell wall ultrastructure to bacterial degradation of wood. *IAWA J.* **2019**, *40*, 845–870. [CrossRef]

25. Rhim, J.W.; Lee, J.H. Thermodynamic Analysis of Water Vapor Sorption Isotherms and Mechanical Properties of Selected Paper-Based Food Packaging Materials. *J. Food Sci.* **2009**, *74*, E502–E511. [CrossRef] [PubMed]

26. Zhang, X.; Li, J.; Yu, Y.; Wang, H. Investigating the water vapor sorption behavior of bamboo with two sorption models. *J. Mater. Sci.* **2018**, *53*, 8241–8249. [CrossRef]

27. Deng, Q. *The Investigation and Excavation of Xiaobaijiao No. I Shipwreck Site of Qing Dynasty in East Sea of China, in Early Navigation in the Asia-Pacific Region*; Springer: Berlin/Heidelberg, Germany, 2016; pp. 241–269.

28. Han, L.; Tian, X.; Zhou, H.; Yin, Y.; Guo, J. The Influences of the Anatomical Structure and Deterioration State of Wood from a Qing Dynasty Shipwreck on Wood Color after the Consolidation Treatment. *J. Southwest Forst. Univ. (Nat. Sci.)* **2020**, *40*, 1–7.

29. Grönquist, P.; Frey, M.; Keplinger, T.; Burgert, I. Mesoporosity of Delignified Wood Investigated by Water Vapor Sorption. *ACS Omega* **2019**, *4*, 12425–12431. [CrossRef] [PubMed]

30. Timmermann, E.O. Multilayer sorption parameters: BET or GAB values? *Colloids Surf. A Physicochem. Eng. Asp.* **2003**, *220*, 235–260. [CrossRef]

31. Wolf, W.; Spiess, W.; Jung, G. *Standardization of Isotherm Measurements (COST-Project 90 and 90 bis), in Properties of Water in Foods*; Springer: Berlin/Heidelberg, Germany, 1985; pp. 661–679.

32. Majka, J.; Babiński, L.; Olek, W. Sorption isotherms of waterlogged subfossil Scots pine wood impregnated with a lactitol and trehalose mixture. *Holzforschung* **2017**, *71*, 813–819. [CrossRef]

33. Basu, S.; Shivhare, U.; Mujumdar, A. Models for sorption isotherms for foods: A review. *Dry. Technol.* **2006**, *24*, 917–930. [CrossRef]

34. Kozłowska, A.; Kozłowski, R. Analysis of water adsorption by wood using the Guggenheim-Anderson-de Boer equation. *Eur. J. Wood Prod.* **2012**, *70*, 445–451.

35. Furmaniak, S.; Terzyk, A.P.; Gauden, P.A.; Rychlicki, G. Applicability of the generalised D'Arcy and Watt model to description of water sorption on pineapple and other foodstuffs. *J. Food Eng.* **2007**, *79*, 718–723. [CrossRef]

36. Sluiter, A.; Hames, B.; Ruiz, R.; Scarlata, C.; Sluiter, J.; Templeton, D.; Crocker, D. Determination of structural carbohydrates and lignin in biomass. *Lab. Anal. Proced.* **2008**, *1617*, 1–16.

37. Han, L.; Wang, K.; Wang, W.; Guo, J.; Zhou, H. Nanomechanical and Topochemical Changes in Elm Wood from Ancient Timber Constructions in Relation to Natural Aging. *Materials* **2019**, *12*, 786. [CrossRef] [PubMed]

38. Thybring, E.E.; Thygesen, L.G.; Burgert, I. Hydroxyl accessibility in wood cell walls as affected by drying and re-wetting procedures. *Cellulose* **2017**, *24*, 2375–2384. [CrossRef]

39. Popescu, C.-M.; Hill, C.A.S.; Curling, S.; Ormondroyd, G.; Xie, Y. The water vapour sorption behaviour of acetylated birch wood: How acetylation affects the sorption isotherm and accessible hydroxyl content. *J. Mater. Sci.* **2013**, *49*, 2362–2371. [CrossRef]

40. Thommes, M.; Kaneko, K.; Neimark, A.V.; Olivier, J.P.; Rodriguez-Reinoso, F.; Rouquerol, J.; Sing, K.S. Physisorption of gases, with special reference to the evaluation of surface area and pore size distribution (IUPAC Technical Report). *Pure Appl. Chem.* **2015**, *87*, 1051–1069. [CrossRef]

41. Broda, M.; Majka, J.; Olek, W.; Mazela, B. Dimensional stability and hygroscopic properties of waterlogged archaeological wood treated with alkoxysilanes. *Int. Biodeter. Biodegr.* **2018**, *133*, 34–41. [CrossRef]

42. Brunauer, S.; Deming, L.S.; Deming, W.E.; Teller, E. On a theory of the van der Waals adsorption of gases. *J. Am. Chem. Soc.* **1940**, *62*, 1723–1732. [CrossRef]

43. Popescu, C.-M.; Hill, C.A.; Kennedy, C. Variation in the sorption properties of historic parchment evaluated by dynamic water vapour sorption. *J. Cult.* **2016**, *17*, 87–94. [CrossRef]

44. Engelund, E.T.; Thygesen, L.G.; Svensson, S.; Hill, C.A.S. A critical discussion of the physics of wood–water interactions. *Wood Sci. Technol.* **2012**, *47*, 141–161. [CrossRef]

45. Fredriksson, M.; Thybring, E.E. Scanning or desorption isotherms? Characterising sorption hysteresis of wood. *Cellulose* **2018**, *25*, 4477–4485. [CrossRef]

46. Olek, W.; Majka, J.; Stempin, A.; Sikora, M.; Zborowska, M. Hygroscopic properties of PEG treated archaeological wood from the rampart of the 10th century stronghold as exposed in the Archaeological Reserve Genius loci in Poznań (Poland). *J. Cult.* **2016**, *18*, 299–305. [CrossRef]

47. Broda, M.; Curling, S.F.; Spear, M.J.; Hill, C.A.S. Effect of methyltrimethoxysilane impregnation on the cell wall porosity and water vapour sorption of archaeological waterlogged oak. *Wood Sci. Technol.* **2019**, *53*, 703–726. [CrossRef]

48. Esteban, L.G.; Simón, C.; Fernández, F.G.; de Palacios, P.; Martín-Sampedro, R.; Eugenio, M.E.; Hosseinpourpia, R. Juvenile and mature wood of Abies pinsapo Boissier: Sorption and thermodynamic properties. *Wood Sci. Technol.* **2015**, *49*, 725–738. [CrossRef]

49. De Oliveira, G.H.H.; Corrêa, P.C.; de Oliveira, A.P.L.R.; Reis, R.C.d.; Devilla, I.A. Application of GAB model for water desorption isotherms and thermodynamic analysis of sugar beet seeds. *J. Food Process Eng.* **2017**, *40*, e12278. [CrossRef]

50. Lewicki, P.P. The applicability of the GAB model to food water sorption isotherms. *Int. J. Food Sci.* **1997**, *32*, 553–557. [CrossRef]

51. Maskan, M.; Göğüş, F. The fitting of various models to water sorption isotherms of pistachio nut paste. *J. Food Eng.* **1997**, *33*, 227–237. [CrossRef]

52. Salmén, L.; Burgert, I. Cell wall features with regard to mechanical performance. A review COST Action E35 2004–2008: Wood machining—Micromechanics and fracture. *Holzforschung* **2009**, *63*, 121–129. [CrossRef]

53. Pettersen, R.C. *The Chemical Composition of Wood*; ACS Publications: Washington, DC, USA, 1984.

54. Xia, Y.; Chen, T.Y.; Wen, J.L.; Zhao, Y.L.; Qiu, J.; Sun, R.C. Multi-analysis of chemical transformations of lignin macromolecules from waterlogged archaeological wood. *Int. J. Biol. Macromol.* **2017**, *109*, 407–416. [CrossRef]

55. Altgen, M.; Willems, W.; Hosseinpourpia, R.; Rautkari, L. Hydroxyl accessibility and dimensional changes of Scots pine sapwood affected by alterations in the cell wall ultrastructure during heat-treatment. *Polym. Degrad. Stabil.* **2018**, *152*, 244–252. [CrossRef]

56. Hill, C.A. *Wood Modification: Chemical, Thermal and Other Processes*; John Wiley & Sons: Hoboken, NJ, USA, 2007; Volume 5.

57. Zelinka, S.L. Preserving ancient artifacts for the next millennia. *Proc. Natl. Acad. Sci. USA* **2014**, *111*, 17700–17701. [CrossRef]

58. Popescu, C.-M.; Dobele, G.; Rossinskaja, G.; Dizhbite, T.; Vasile, C. Degradation of lime wood painting supports. *J. Anal. Appl. Pyrol.* **2007**, *79*, 71–77. [CrossRef]

59. Popescu, C.-M.; Hill, C.A.S. The water vapour adsorption–desorption behaviour of naturally aged Tilia cordata Mill. wood. *Polym. Degrad. Stabil.* **2013**, *98*, 1804–1813. [CrossRef]

60. Rautkari, L.; Hill, C.A.; Curling, S.; Jalaludin, Z.; Ormondroyd, G. What is the role of the accessibility of wood hydroxyl groups in controlling moisture content? *J. Mater. Sci.* **2013**, *48*, 6352–6356. [CrossRef]

61. Guo, X.; Liu, L.; Hu, Y.; Wu, Y. Water vapor sorption properties of TEMPO oxidized and sulfuric acid treated cellulose nanocrystal films. *Carbohydr. Polym.* **2018**, *197*, 524–530. [CrossRef] [PubMed]

62. Sharma, P.R.; Joshi, R.; Sharma, S.K.; Hsiao, B.S. A simple approach to prepare carboxycellulose nanofibers from untreated biomass. *Biomacromolecules* **2017**, *18*, 2333–2342. [CrossRef] [PubMed]

63. Klemm, D.; Heublein, B.; Fink, H.P.; Bohn, A. Cellulose: Fascinating biopolymer and sustainable raw material. *Angew. Chem. Int. Ed.* **2005**, *44*, 3358–3393. [CrossRef] [PubMed]

64. Hofstetter, K.; Hinterstoisser, B.; Salmén, L. Moisture uptake in native cellulose–the roles of different hydrogen bonds: A dynamic FT-IR study using Deuterium exchange. *Cellulose* **2006**, *13*, 131–145. [CrossRef]

65. Fernandes, A.N.; Thomas, L.H.; Altaner, C.M.; Callow, P.; Forsyth, V.T.; Apperley, D.C.; Kennedy, C.J.; Jarvis, M.C. Nanostructure of cellulose microfibrils in spruce wood. *Proc. Natl. Acad. Sci. USA* **2011**, *108*, 1195–1203. [CrossRef]

66. Šturcová, A.; His, I.; Apperley, D.C.; Sugiyama, J.; Jarvis, M.C. Structural details of crystalline cellulose from higher plants. *Biomacromolecules* **2004**, *5*, 1333–1339. [CrossRef]

67. Eyley, S.; Thielemans, W. Surface modification of cellulose nanocrystals. *Nanoscale* **2014**, *6*, 7764–7779. [CrossRef]

68. Mihranyan, A.; Llagostera, A.P.; Karmhag, R.; Strømme, M.; Ek, R. Moisture sorption by cellulose powders of varying crystallinity. *Int. J. Pharm.* **2004**, *269*, 433–442. [CrossRef] [PubMed]

69. Han, L.; Tian, X.; Keplinger, T.; Zhou, H.; Li, R.; Svedström, K.; Burgert, I.; Yin, Y.; Guo, J. Even Visually Intact Cell Walls in Waterlogged Archaeological Wood Are Chemically Deteriorated and Mechanically Fragile: A Case of a 170 Year-Old Shipwreck. *Molecules* **2020**, *25*, 1113. [CrossRef] [PubMed]

70. Colombini, M.P.; Lucejko, J.J.; Modugno, F.; Orlandi, M.; Tolppa, E.L.; Zoia, L. A multi-analytical study of degradation of lignin in archaeological waterlogged wood. *Talanta* **2009**, *80*, 61–70. [CrossRef] [PubMed]

71. Pedersen, N.B.; Gierlinger, N.; Thygesen, L.G. Bacterial and abiotic decay in waterlogged archaeological Picea abies (L.) Karst studied by confocal Raman imaging and ATR-FTIR spectroscopy. *Holzforschung* **2015**, *69*, 103–112. [CrossRef]